

Confirmation of interstellar phosphine towards asymptotic giant branch star IRC+10216

Arijit Manna¹, Sabyasachi Pal^{1,*}

¹Department of Physics and Astronomy, Midnapore City College, Paschim Medinipur, West Bengal, India 721129

*Corresponding author. E-mail: sabya.pal@gmail.com

Abstract. Phosphorus (P) is an important element for the chemical evolution of galaxies and many kinds of biochemical reactions. Phosphorus is one of the crucial chemical compounds in the formation of life on our planet. In an interstellar medium, phosphine (PH₃) is a crucial biomolecule that plays a major role in understanding the chemistry of phosphorus-bearing molecules, particularly phosphorus nitride (PN) and phosphorus monoxide (PO), in the gas phase or interstellar grains. We present the first confirmed detection of phosphine (PH₃) in the asymptotic giant branch (AGB) carbon-rich star IRC+10216 using the Atacama Large Millimeter/Submillimeter Array (ALMA) band 6. We detect the $J = 1_0-0_0$ rotational transition line of PH₃ with a signal-to-noise ratio (SNR) of $\geq 3.5\sigma$. This is the first confirmed detection of phosphine (PH₃) in the ISM. Based on LTE spectral modelling, the column density of PH₃ is $(3.15 \pm 0.20) \times 10^{15} \text{ cm}^{-2}$ at an excitation temperature of $52 \pm 5 \text{ K}$. The fractional abundance of PH₃ with respect to H₂ is $(8.29 \pm 1.37) \times 10^{-8}$. We also discuss the possible formation pathways of PH₃ and we claim that PH₃ may be created via the hydrogenation of PH₂ on the grain surface of IRC+10216.

Keywords. ISM: individual objects (IRC+10216) – ISM: abundances – ISM: kinematics and dynamics – stars: formation – astrochemistry

1. Introduction

Phosphorus is one of the rare elements in the interstellar medium (ISM). Phosphorus is the 13th element in the meteoritic material and the 11th element in the crust of Earth (Maciá et al., 1997). In ISM, the prebiotic chemistry of phosphorus (P) has attracted attention in astrochemical communities because P-bearing molecules, such as phosphorus monoxide (PO) and phosphorus nitride (PN), play important roles in the production of phospholipids and nucleic acids (Turner et al., 1990; Fontani et al., 2016). Phospholipids and nucleic acids are important for the formation of life on our planet. P-bearing molecules may play an important role in the production of large complex biomolecules that store genetic information in nucleic acids (Maciá et al., 1997). P-bearing molecules also play major roles in the synthesis of DNA and RNA (Maciá et al., 1997). Earlier millimeter and submillimeter wavelength observations indicated the depletion of P-bearing molecules by a factor of ≥ 100 with respect to the cosmic abundance of P ($\sim 3 \times 10^{-7}$) in cold and dense parts of the ISM (Turner et al., 1990; Fontani et al., 2016; Lefloch et al., 2016). The depletion of P-bearing molecules suggests that the bulk of P-bearing species is blocked by interstellar grains (Fontani et al., 2016). Recently,

the ESA Probe Rosetta and the ALMA demonstrated that P-bearing species came to Earth through comets (Altwegg et al., 2016; Rivilla et al., 2020). Comets carry several biomolecules because they travel between several star-forming regions (Altwegg et al., 2016). In ISM, P-bearing molecules, such as PO, PN, HCP, CCP, and CP, were detected in the envelopes around evolved stars (Guélin et al., 1990; Tenenbaum et al., 2007; Halfen et al., 2008; Milam et al., 2008; Tenenbaum et al., 2008; De Beck et al., 2013; Ziurys et al., 2018).

In ISM, phosphine (PH₃) is a relatively stable oblate symmetric top molecule. The rotational levels of PH₃ are given by two quantum numbers (J, K), and radiative transitions are allowed within the levels of the K ladder ($\Delta J = 1, \Delta K = 0$). The electric dipole moment of PH₃ is 0.573 Debye (Davies et al., 1971). Sousa-Silva et al. (2020) claimed that PH₃ acts as a biosignature in the space. Except for our planet, evidence of PH₃ is also found in the atmospheres of Saturn and Jupiter with mixing ratios of 2 ppm and 0.6 ppm using the Voyager data (Maciá et al., 2005). Subsequently, Fletcher et al. (2009) demonstrated the global distribution of PH₃ in the atmosphere of Saturn and Jupiter by using Cassini/CIRS observations. Recently, Gapp et al. (2024) also found evidence of PH₃ in the atmosphere of Jupiter using Herschel/PACS. At high tem-

Table 1: Stellar properties of IRC+10216.

Physical properties	Value	Ref
α (J2000)	09:47:57.4	SIMBAD data base
δ (J2000)	+13:16:43.5	SIMBAD data base
Distance	130 pc	Menten et al. (2012)
Pulsation period	639±4 days	Groenewegen et al. (2012)
T_{eff}	~2200 K	Menten et al. (2012)
Photospheric diameter (optical)	3.8 AU	Menten et al. (2012)
Luminosity	8640±430 L_{\odot}	Menten et al. (2012)
Initial mass	3–5 M_{\odot}	Guélin et al. (1995)
Current mass	0.7–0.9 M_{\odot}	Ladjal et al. (2010)
Mass-loss	$2 \times 10^{-5} M_{\odot} \text{ yr}^{-1}$	Crosas & Menten (1997)
V_{outflow}	14.6±0.3 km s ⁻¹	Knapp et al. (1998)
V_{LSR}	-26±0.3 km s ⁻¹	Knapp et al. (1998)

peratures and pressures, PH₃ is produced in the deep atmosphere on large gas planets ([Bregman et al., 1975](#); [Tarrago et al., 1992](#)). Recently, [Greaves et al. \(2021\)](#) reported the identification of the absorption line of PH₃ at a frequency of 266.944 GHz using ALMA and JCMT on the deck of Venus with a mixing ratio of 20 ppb. Several questions exist regarding the detection of PH₃ and the chemical models of the atmosphere of Venus. First, [Greaves et al. \(2021\)](#) could not explain the formation of highly abundant PH₃ in the atmosphere of Venus by using steady-state and photochemical models. [Greaves et al. \(2021\)](#) showed different abiotic chemical routes to explain the high abundance of PH₃ in the atmosphere of Venus. Subsequently, [Villanueva et al. \(2021\)](#) and several other authors raised questions regarding the spectroscopic data analysis by [Greaves et al. \(2021\)](#). [Villanueva et al. \(2021\)](#) and other authors clearly showed there is no evidence of PH₃ in the atmosphere of Venus. Subsequently, [Cordiner et al. \(2022\)](#) also attempted to search for the emission lines of other transitions of PH₃ at frequencies of 533 GHz and 1067 GHz using the NASA SOFIA aircraft, but they could not detect any absorption lines of PH₃. Therefore, [Cordiner et al. \(2022\)](#) estimated that the upper limit of PH₃ in Venus in the altitude range of 75–110 km is ≤0.8 ppb. Earlier, [Olsen et al. \(2021\)](#) also searched for evidence of PH₃ towards the atmosphere of Mars, but they did not detect PH₃. The upper limit abundance of PH₃ towards Mars is ≤0.6 ppbv ([Olsen et al., 2021](#)). Except for our solar system, the emission line of PH₃ was tentatively detected in the envelope of the carbon-rich star IRC+10216 using the IRAM 30 m single-dish telescope ([Agúndez et al., 2008](#)). This detection is tentative because [Agúndez et al. \(2008\)](#) did not properly

identify the emission line of PH₃ at 266.944 GHz, owing to the limitation of the spectral resolution (~1.25 MHz) of IRAM. [Agúndez et al. \(2008\)](#) also claimed that IRC+10216 is one of the sources in the ISM where a very high abundance of PH₃ is still present because the PH₃/HCP abundance ratio is similar to the NH₃/HCN in the envelope of this source.

IRC+10216 (alternatively CW Leonis) is known as a carbon-rich asymptotic giant branch (AGB) star located at a distance of 130 pc ([Menten et al., 2012](#)). This carbon-rich star is near the end of its evolution and is very close to being converted into a protoplanetary nebula ([Skinner et al., 1998](#); [Osterbart et al., 2000](#)). The physical properties of IRC+10216 are presented in Table 1. IRC+10216 loses mass at a very high rate ($2 \times 10^{-5} M_{\odot} \text{ yr}^{-1}$) because the object is very close to the end of its AGB lifetime and this source is covered by an extensive circumstellar envelope (CSE) ([Crosas & Menten, 1997](#)). This source is ideal for studying complex organic molecular lines because of its carbon-rich environment. Approximately 70 individual molecules have been detected in IRC+10216, including MgNC, AlNC, NaCN, AlCl, NaCl, KCl, AlF, and carbon-chain molecules ([Cernicharo & Guélin, 1987](#); [Cernicharo et al., 2000](#); [Ziurys et al., 2002](#)).

In this letter, we present the first confirmation of interstellar phosphine (PH₃) towards the carbon-rich star IRC+10216 using ALMA. For the detection of the emission line of PH₃, we used the local thermodynamic equilibrium model (LTE). The observations and data reduction are presented in Section 2.. The result of the detection of the rotational emission line of PH₃ is shown in Section 3.. The discussion and conclusion are shown in Section 4. and 5..

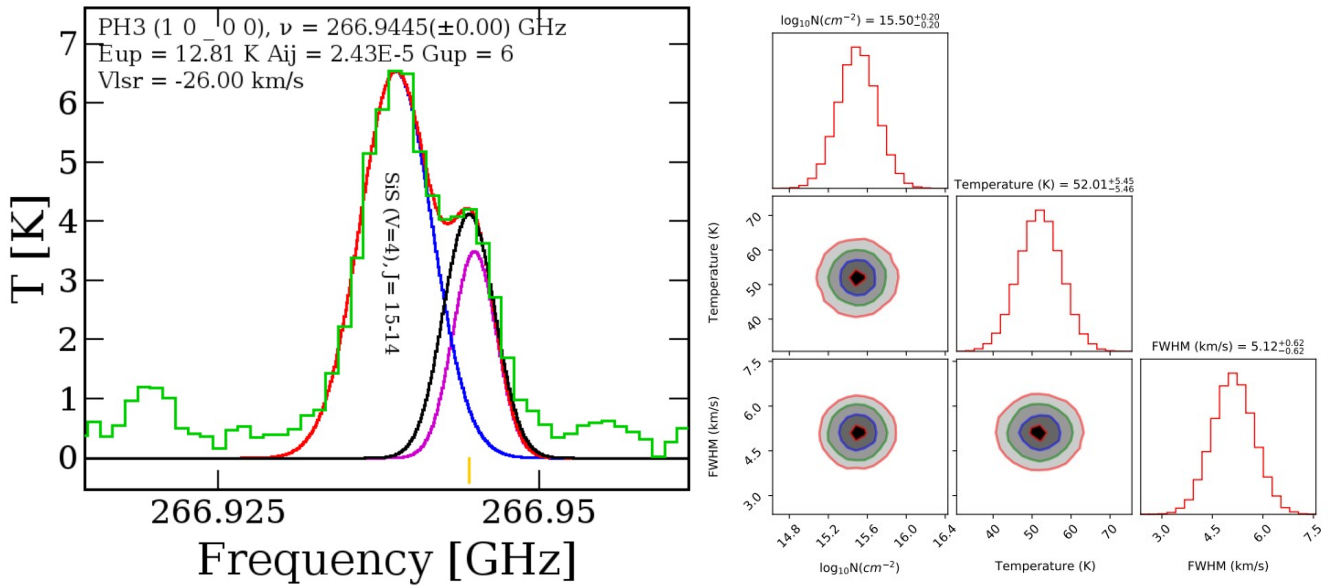


Figure 1: Rotational emission line of PH₃ with transition $J = 1_0-0_0$ towards IRC+10216 (left panel). The green lines represent the observed molecular spectrum of IRC+10216. The black spectra indicate the best-fit LTE model spectra for PH₃. The red spectrum is the global Gaussian model. The blue spectra are the Gaussian model corresponding to the SiS ($V = 4$) emission line, and the violet spectra are the Gaussian model corresponding to the PH₃ emission line. The yellow vertical line indicates the rest frequency position of the PH₃. The right panel image shows the corner diagram plot based on MCMC fittings. Corner plots showing the 3D posterior probability distributions of column density in cm^{-2} , excitation temperature in K, and FWHM in km s^{-1} .

2. Observations and data reductions

We used the cycle 0 archival data of IRC+10216, which was observed using a high-resolution ALMA in band 6 (PI: Cernicharo, Jose, ID: 2011.0.00229.S) with a 12 m array. This observation was performed on April 8, 2012, to study the emission lines of HCN with transitions $J = 3-2$ and $J = 8-7$ and observation of the dust formation zone in IRC+10216 with an on-source integration time of 32.76 min. The phase centre of IRC+10216 observation was $(\alpha, \delta)_{J2000} = 09:47:57.406, +13:16:43.561$. At the time of observation, 3C 279 and 3C 273 were used as bandpass and flux calibrators, respectively. J0854+201 was used as the phase calibrator. During the observation period, 16 antennas were used, with a minimum baseline of 15.7 m and a maximum baseline of 384.1 m. Observations were performed in the frequency ranges of 265.05–266.92 GHz, 266.15–268.03 GHz, 267.54–269.42 GHz, and 268.05–269.92 GHz with a spectral resolution of 976.56 kHz.

For data analysis, we used the Common Astronomy Software Application (CASA 5.4.1) with the ALMA data analysis pipeline (McMullin et al., 2007). We applied the Perley-Butler 2017 flux calibration model for each baseline for flux calibration using the SETJY task (Perley & Butler, 2017). We also used the pipeline tasks HIFA_bandpassflag and HIFA_flagdata for flag-

ging bad antenna data and channels, which were performed after flux and bandpass calibration. After a preliminary reduction of the data, we split the target data (IRC+10216) using the MSTRANSFORM task with all the rest frequencies. We also used the UVCNTSUB task to subtract continuum emission from the UV plane of the calibrated data. After data reduction, continuum emission images of IRC+10216 were created using the TCLEAN task with a HOGBOM deconvolver for line-free channels. Earlier, Agúndez et al. (2015) discussed the dust continuum emission of IRC+10216 using the same data. Therefore, we do not discuss dust continuum emissions in this study. We also created spectral data cubes using the TCLEAN task with the SPECMODE = CUBE parameter and Briggs weighting with a robust value of 0.5. We also applied a multiple self-calibration method to improve the RMS of the data cubes. To correct the primary beam pattern, we used the IMPBCOR task.

3. Result

3.1 Identification of PH₃ towards IRC+10216

To study the rotational emission line of PH₃, we only focus on the spectral data cube that was observed between the frequency range of 266.15 GHz and 268.03 GHz because the rest frequency of PH₃ ($J = 1_0-0_0$)

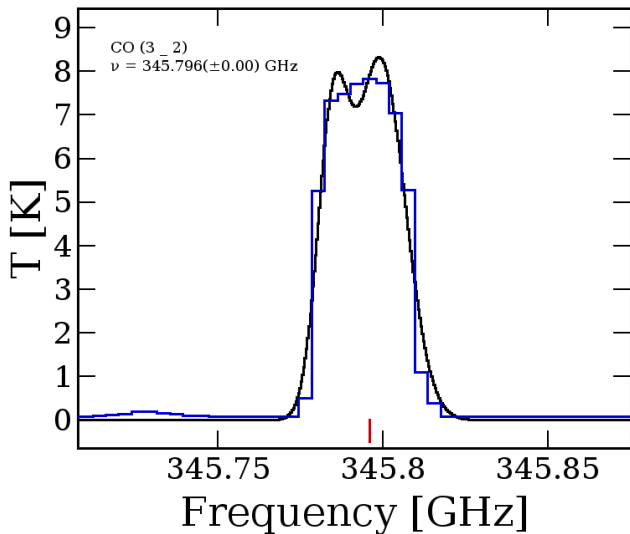


Figure 2: Rotational emission line of carbon monoxide (CO) with transition $J = 3-2$ towards IRC+10216. The blue line indicates the observed spectra of CO, and the black spectrum is the best-fitting Gaussian model.

is 266.944 GHz. We extracted the molecular spectra of IRC+10216 from the spectral data cube to create a $2.3''$ diameter circular region over the line-emitting region of the source, which is larger than the synthesized beam size of the spectral data cube. The synthesized beam size of the spectral data cube is $0.90'' \times 0.48''$. The systemic velocity (V_{LSR}) of IRC+10216 is -26.5 km s^{-1} (Agúndez et al., 2015). To identify the rotational emission line of PH_3 , we used the local thermodynamic equilibrium (LTE) model spectra with the Cologne Database for Molecular Spectroscopy (CDMS) database (Müller et al., 2005). To fit the LTE spectra to the observed spectra of PH_3 , we used the Markov chain Monte Carlo (MCMC) algorithm in CASSIS (Vastel et al., 2015). The MCMC analysis using the CASSIS is well described in Manna & Pal (2024). The MCMC method initializes by randomly selecting a seed point (X_0) in the three-dimensional parameter space. Then, it randomly chooses a nearby point (X_1) based on a variable step size, which is recalculated for each iteration. The χ^2 value of the new state (X_1) is calculated, and if the ratio $p = \chi^2(X_0)/\chi^2(X_1) > 1$, the new state is accepted. However, even if $p < 1$, the new state may still be accepted with a certain probability. If the new state is rejected, the original state (X_0) remains, and another nearby point (X_1) is randomly selected. By allowing a finite probability of accepting a worse χ^2 value, the algorithm avoids converging directly to a local minimum and instead ensures a more thorough exploration of the entire parameter space. During our MCMC analysis, we employed 1000 walkers, uniformly distributed within the specified parameter ranges, and ran the chains

for a burning sequence of 20,000 steps to ensure convergence. The MCMC approach allows us to vary all parameters, including column density, excitation temperature, and full width at half maximum (FWHM) until the best fit is obtained. After the LTE spectral analysis, we detected the emission line of PH_3 at a frequency of 266.944 GHz with transition $J = 1_0-0_0$ in the spectra of IRC+10216. We also observed that the emission line of PH_3 is closely associated with the emission line of SiS $V = 4$ with transition $J = 15-14$. The rest frequency of the emission line of SiS $V = 4$ is 266.941 GHz, which was obtained from Agúndez et al. (2008). Previously, Agúndez et al. (2008) and Agúndez et al. (2014) attempted to search the emission line of PH_3 ($J = 1_0-0_0$) using the IRAM 30 m telescope, but the authors did not detect the proper peak of the emission line of PH_3 because of the limitation in the resolution of the IRAM. Our detection of the emission line of PH_3 using ALMA is the first confirmation of the presence of PH_3 in IRC+10216. After spectral analysis, we see that the emission line of PH_3 is non-blended. The upper state energy (E_u) and Einstein coefficients (A_{ij}) of the identified PH_3 transition are 12.81 K and $2.43 \times 10^{-5} \text{ s}^{-1}$. The full-width half maximum (FWHM) of the LTE spectra is $5.12 \pm 0.62 \text{ km s}^{-1}$. According to the LTE model, the best-fit column density of PH_3 is $(3.15 \pm 0.20) \times 10^{15} \text{ cm}^{-2}$ with an excitation temperature of $52 \pm 5 \text{ K}$ and a source size of $0.90''$. Our estimated excitation temperature of PH_3 is similar to the excitation temperature of another P-bearing molecule, CP, which was estimated by Milam et al. (2008). The excitation temperature of PH_3 is relatively low because the AGB star is near the end of its evolution. The peak and integrated intensities of the detected emission line of PH_3 are $4.26 \pm 0.12 \text{ K}$ and $20.46 \pm 0.56 \text{ K km s}^{-1}$ respectively. The optical depth of the spectra of PH_3 is 5.81×10^{-2} . The estimated optical depth indicates that the identified rotational emission line of PH_3 is optically thin. The LTE-fitted rotational emission line of PH_3 towards IRC+10216 is shown in Figure 1. In addition, we created a corner plot corresponding to the LTE fitting values. The corner plot shows the 3D posterior probability distributions of column density in cm^{-2} , excitation temperature in K, and FWHM in km s^{-1} of PH_3 towards IRC+10216, which is shown in the right panel of Figure 1.

3.2 Estimation of the column density of molecular H_2 towards IRC+10216

To determine the column density of molecular H_2 towards IRC+10216, we used the following equation:

$$N(\text{H}_2) = 2.0 \times 10^{20} \times \frac{W(^{12}\text{CO})}{\text{K km s}^{-1}}, \quad (1)$$

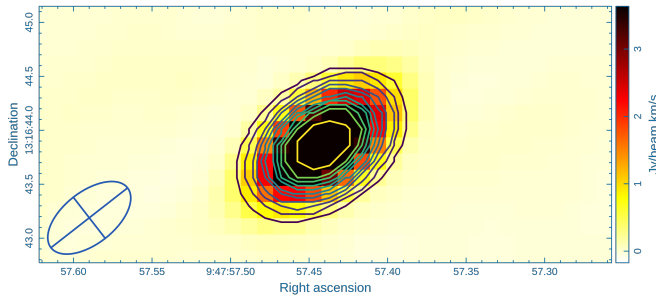


Figure 3: Integrated emission map of PH_3 towards IRC+10216. The contour levels are started at 3σ and are increased by a factor of $\sqrt{2}$. The blue circle represents the synthesized beam of the integrated emission map.

where $W(^{12}\text{CO})$ is the integrated intensity of ^{12}CO ($J = 3-2$) at the corresponding velocity intervals. This equation was taken from Isequilla et al. (2021). To determine the emission line properties of CO, we used the 2016.1.00251.S (PI: Vlemmings Wouter) ALMA data. The analysis of this ALMA data is well described in Siebert et al. (2022). The emission line of CO towards IRC+10216 is shown in Figure 2. We fitted a Gaussian model over the emission line of CO and estimated that the integrated intensity of the CO line is $190.39 \text{ K km s}^{-1}$. Using the above equation, the estimated column density of H_2 towards IRC+10216 is $(3.80 \pm 0.58) \times 10^{22} \text{ cm}^{-2}$.

3.3 Abundance of PH_3 towards IRC+10216

To derive the fractional abundance of PH_3 , we used the column density of PH_3 inside the $0.90''$ synthesized beam, which was divided by the column density of H_2 . The fractional abundance of PH_3 with respect to molecular H_2 towards IRC+10216 is $(8.29 \pm 1.37) \times 10^{-8}$, where the column density of molecular H_2 towards IRC+10216 is $(3.80 \pm 0.58) \times 10^{22} \text{ cm}^{-2}$. Previously, Agúndez et al. (2008) and Agúndez et al. (2014) estimated the tentative abundance of PH_3 towards IRC+10216, which varied between $\sim 10^{-9}$ and $\sim 10^{-8}$. Our estimated fractional abundance of PH_3 using ALMA data is similar to those of Agúndez et al. (2014) but one order of magnitude higher than those of Agúndez et al. (2008). Previously, Lefloch et al. (2016) attempted to detect the emission line of PH_3 at a frequency of 266.944 GHz using the IRAM 30 m telescope towards the solar-type star-forming region L1157, however, they could not successfully detect the emission line of PH_3 . The upper limit of the abundance of PH_3 towards L1157 is $\leq 10^{-9}$ (Lefloch et al., 2016). Recently, Furuya & Shimonishi (2024) also searched the emission line of PH_3 ($J = 1_0-0_0$) towards L1544 using the ALMA, but they could

not detect PH_3 . The upper limit column density and abundance of PH_3 towards L1544 are $\leq 7.6 \times 10^{10} \text{ cm}^{-2}$ and $\leq 6.7 \times 10^{-12}$, respectively (Furuya & Shimonishi, 2024). Therefore, we confirm that IRC+10216 is the only source in the ISM where evidence of PH_3 is found.

3.4 Spatial distribution of PH_3

We created an integrated emission map of PH_3 ($J = 1_0-0_0$) towards IRC+10216 using the IMMOMENTS task. In the IMMOMENTS task, we used the channel ranges of the spectral data cubes, where the emission lines of PH_3 were identified. The integrated emission map of PH_3 is shown in Figure 3. The emission map clearly shows that the emission line of PH_3 originated from the inner envelope of IRC+10216. We also fitted a 2D Gaussian over the integrated emission map of PH_3 using the IMFIT task. The following equation is used to estimate the emitting region of PH_3

$$\theta_s = \sqrt{\theta_{50}^2 - \theta_{\text{beam}}^2} \quad (2)$$

In the above equation, $\theta_{50} = 2\sqrt{A/\pi}$ indicates the diameter of the circle whose area (A) surrounds the 50% line peak of PH_3 and θ_{beam} indicates the half-power width of the synthesized beam of the integrated emission map of PH_3 (Manna et al., 2023). The size of the emitting region of PH_3 is $0.83''$. The synthesized beam size of the integrated emission map of PH_3 is $0.90'' \times 0.48''$. We observed that the emitting region of PH_3 is slightly smaller than the synthesized beam size of the integrated emission map. This indicates that the detected emission line of PH_3 is not spatially resolved towards IRC+10216. Therefore, we cannot draw any conclusions regarding the spatial distribution morphology of PH_3 towards IRC+10216. Higher angular and spatial resolution observations with better spectral resolution are required to understand the chemical morphology of PH_3 towards IRC+10216.

4. Discussion

4.1 Possible formation mechanism of PH_3

Previous chemical modelling studies have indicated that PH_3 is an important biomolecule that plays a major role in the production of other P-bearing molecules using the surface chemistry of the interstellar grains (Charnley & Millar, 1994; Aota & Aikawa, 2012; Nguyen et al., 2020). Earlier, Nguyen et al. (2020) showed that PH_3 is created on the grain surface rather than in the gas phase. Charnley & Millar (1994) and Nguyen et al. (2020) proposed a possible formation mechanism for

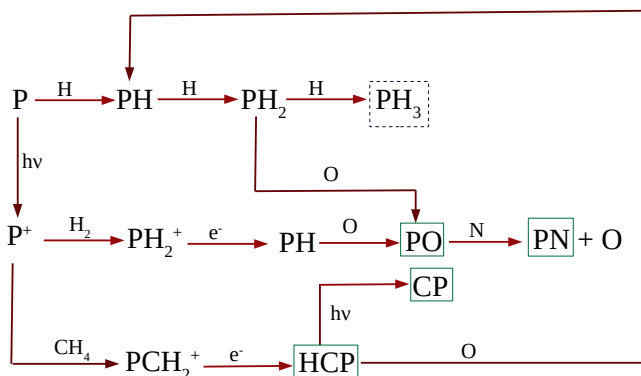
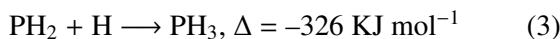
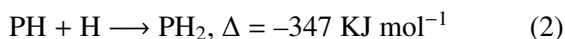


Figure 4: The proposed gas phase and grain surface chemical network for the formation of PH_3 and link with other P-bearing molecules. The green box indicates P-bearing molecules which were previously detected in IRC+10216.

PH_3 via the hydrogenation of atomic P on the grain surface of the highly dense part of star-formation regions and hot molecular cores via the following reactions.



Since reactions 1–3 are barrierless, PH_3 can be produced on the grain surface. At low temperatures (~ 10 K), the hydrogen atom (H) can diffuse and react with other compounds on the grain surface (Hama & Watanabe, 2013). Previously, no P-bearing molecules, including PH_3 , were observed in the solid state. Turner et al. (2015, 2018, 2019) experimentally observed that solid PH_3 is converted into phosphoric acid, diphosphate, and methyl phosphonic acid at low temperatures. Chantzios et al. (2020) also showed that the PH_3 is destroyed due to the reaction of C^+ ($\text{C}^+ + \text{PH}_3 \longrightarrow \text{PH}_3^+ + \text{C}$) and H^+ ($\text{H}^+ + \text{PH}_3 \longrightarrow \text{PH}_3^+ + \text{H}$). Earlier, Agúndez et al. (2014) computed the chemical model of PH_3 in the IRC +10216 environment using reaction 3, and they found that the model abundance of PH_3 is 1.0×10^{-8} . Our observed abundance of PH_3 towards IRC+10216 using the ALMA is very close to the modelled abundance of PH_3 , which was estimated by Agúndez et al. (2014). This indicates PH_3 is formed via hydrogenation of PH_2 on the grain surface of IRC+10216.

4.2 Chemical link-up between PH_3 and other molecules

Previously the emission lines of HCP, CP, PO, and PN were detected towards the IRC+10216 (Matthews et al.,

1987; Guélin et al., 1990; Milam et al., 2008). We created a chemical network to understand the prebiotic chemistry of PH_3 and the chemical link-up between all detected P-bearing species towards IRC+10216, as shown in Figure 4. The chemical reactions are taken from Charnley & Millar (1994), Aota & Aikawa (2012), Hama & Watanabe (2013), Nguyen et al. (2020), and UMIST 2012 (McElroy et al., 2013) molecular reaction database. Our chemical network clearly shows that PH acts as a possible precursor of PH_3 , PN, and PO. Previously, Agúndez et al. (2014) showed that the gas phase chemistry is not sufficient for the formation of PH_3 . Therefore, there is a high chance of the formation of PH_3 via hydrogenation of PH_2 on the grain surface of IRC+10216. A new chemical model using the gas-grain chemistry and quantum chemical studies using the density functional theory (DFT) is needed with proper formation and destruction pathways of PH_3 with reaction rates to understand the chemical evolution and proper formation and destruction pathways of PH_3 towards IRC+10216.

5. Summary and conclusion

In this letter, we present the first confirmation of the rotational emission line of PH_3 towards the carbon-rich AGB star IRC+10216 at a frequency of 266.944 GHz using the ALMA band 6. The abundance of PH_3 towards IRC+10216 is $(8.29 \pm 1.37) \times 10^{-8}$. We discuss the possible formation pathways of PH_3 and we claim that PH_3 may be formed via the hydrogenation of PH_2 on the grain surface of IRC+10216. The confirmed detection of PH_3 indicates that the grain surface chemistry is sufficient for the production of other P-bearing molecules because PH_3 and PH act as possible precursors of other P-bearing molecules. Our chemical network shows that PH_3 , PN, and PO are chemically connected to the PH. A detailed spectral line study and chemical modelling are required to understand other P-bearing molecules towards IRC+10216, which will be carried out in our next follow-up study.

Acknowledgement

We thank the anonymous referee for the helpful comments that improved the manuscript. A.M. acknowledges the Swami Vivekananda Merit cum Means Scholarship, Government of West Bengal, India, for financial support for this research. The emission spectra of PH_3 are available on our [github](#) repository. The emission map and chemical network of PH_3 within this paper is available from the corresponding author upon reasonable request. This paper makes use of the following

ALMA data: ADS /JAO.ALMA#2011.0.00229.S and 2016.1.00251.S. ALMA is a partnership of ESO, NSF (USA), and NINS (Japan), together with NRC (Canada), MOST and ASIAA (Taiwan), and KASI (Republic of Korea), in cooperation with the Republic of Chile. The JAO is operated by ESO, AUI/NRAO, and NAOJ.

References

- Altwegg, K., Balsiger, H., Bar-Nun, A., et al. 2016, *SciA*, 2, e1600285
- Agúndez, M., Cernicharo, J., Pardo, J. R., Guélin, M., Phillips, T. G., 2008, *A&A*, 485, L33-L36
- Agúndez, M., Cernicharo, J., Decin, L., Encrenaz, P., Teyssier, D., 2014, *ApJL*, 790, 2, L27
- Aota, T., & Aikawa, Y. 2012, *ApJ*, 761, 74
- Agúndez, M., Cernicharo, J., Quintana-Lacaci, G., Velilla Prieto, L., Castro-Carrizo, A., Marcelino, N., Guélin, M. 2015, *ApJ*, 814, 143
- Bregman, J., Lester, D., & Rank, D. 1975, *ApJL*, 202, L55
- Crosas, M., Menten, K., 1997, *ApJ*, 483, 913
- Cordiner, M. A., Villanueva, G. L., Wiesemeyer, H., et al., 2022, *GRL*, 49, 22
- Charnley, S. B., & Millar, T. J. 1994, *MNRAS*, 270, 570
- Chantzios, J., Rivilla, V. M., Vasyunin, A., et al. 2020, *A&A*, 633, A54
- Cernicharo, J., Guélin, M., & Kahane, C. 2000, *A&AS*, 142, 181
- Cernicharo, J., & Guélin, M. 1987, *A&A*, 183, L10
- De Beck, E., Kamiński, T., Patel, N. A., et al. 2013, *A&A*, 558, A132
- Davies, P. B., Neumann, R. M., Wofsy, S. C., & Klemperer, W. 1971, *J. Chem. Phys.*, 55, 3564
- Fontani, F., Rivilla, V. M., Caselli, P., Vasyunin, A., & Palau, A. 2016, *ApJL*, 822, L30
- Fletcher, L. N., Orton, G. S., Teanby, N. A., & Irwin, P. G. J. 2009, *Icarus*, 202, 543
- Furuya, K., & Shimonishi, T., 2024, *ApJL*, 968, L19
- Gapp, C., Rengel, M., Hartogh, P., Sagawa, H., Feuchtgruber, H., Lellouch, E., Villanueva, G. L., 2024, *A&A*, 688, A10
- Groenewegen M. A. T. et al., 2012, *A&A*, 543, L8
- Guélin M., Forestini M., Valiron P., Ziurys L. M., Anderson M. A., Cernicharo J., Kahane C., 1995, *A&A*, 297, 183
- Guélin, M., Cernicharo, J., Paubert, G., & Turner, B. E. 1990, *A&A*, 230, L9-L11
- Greaves, J. S., Richards, A. M. S., Bains, W., et al. 2021, *NatAs*, 5, 655
- Halfen, D. T., Clouthier, D. J., & Ziurys, L. M. 2008, *ApJ*, 677, L101
- Hama, T., & Watanabe, N. 2013, *ChRv*, 113, 8783
- Isequilla, N. L., Ortega, M. E., Areal, M. B., Paron, S. 2021, *A&A*, 649, A139
- Knapp, G. R., Young, K., Lee, E., Jorissen, A., 1998, *ApJS*, 117, 209
- Lefloch, B., Vastel, C., Viti, S., et al. 2016, *MNRAS*, 462, 3937
- Ladjal, D. et al., 2010, *A&A*, 518, L141
- Menten K., Reid M. J., Kaminski T., Claussen M. J., 2012, *A&A*, 543, A73
- Maciá, E., Hernández, M., & Oró, J. 1997, *OLEB*, 27, 459
- Milam, S. N., Halfen, D. T., Tenenbaum, E. D., et al. 2008, *ApJ*, 684, 618
- Maciá, E. 2005, *Chem. Soc. Rev.*, 34, 691
- McMullin, J. P., Waters, B., Schiebel, D., Young, W., & Golap, K. 2007, in *Astronomical Society of the Pacific Conference Series*, Vol. 376, *Astronomical Data Analysis Software and Systems XVI*, ed. R. A. Shaw, F. Hill, & D. J. Bell, 127
- Müller, H. S. P., Schlemöder, F., Stutzki, J. Winnewisser, G., 2005, *J. Mol. Struct.*, 742, 215
- Manna, A., & Pal, S., 2024, *J. Astrophys. Astron*, 45, 3
- Manna, A., Pal, S., Viti, S., Sinha, S., 2023, *MNRAS*, 525, 2229
- Matthews H. E., Feldman P. A., Bernath P. F., 1987, *ApJ*, 312, 358

- McElroy, D., Walsh, C., Markwick, A. J., Cordiner, M. A., Smith K., Millar, T. J., 2013, *A&A*, 550, A36
- Nguyen, T., Oba, Y., Shimonishi, T., Kouchi, A., Watanabe, N. 2020, *ApJL*, 898, L52
- Osterbart R., Balega Y. Y., Blöcker T., Men'shchikov A. B., Weigelt G., 2000, *A&A*, 357, 169
- Olsen, K. S., Trokhimovskiy, A., Braude, A. S., Korablev, O. I., Fedorova, A. A., Wilson, C. F., Patel, M. R., et al., 2021, *A&A*, 649, L1
- Perley, R. A., Butler, B. J. 2017, *ApJs*, 230, 1538
- Rivilla, V. M., Drozdovskaya, M. N., Altwegg, K., et al. 2020, *MNRAS*, 492, 1180
- Siebert, M A., Van de Sande, M., Millar, T J., Remijan, A J. 2022, *ApJ*, 941, 90
- Skinner C. J., Meixner M., Bobrowsky M., 1998, *MNRAS*, 300, 29
- Sousa-Silva, C., Seager, S., Ranjan, S., et al. 2020, *AsBio*, 20, 235
- Turner, B. E., Tsuji, T., Bally, J., Guelin, M., & Cernicharo, J. 1990, *ApJ*, 365, 569
- Tenenbaum, E. D., Woolf, N. J., & Ziurys, L. M. 2007, *ApJ*, 666, L29
- Tenenbaum, E. D., & Ziurys, L. M. 2008, *ApJ*, 680, L121
- Turner, A. M., Abplanalp, M. J., Bergantini, A., et al. 2019, *SciA*, 5, eaaw4307
- Turner, A. M., Abplanalp, M. J., Chen, S. Y., et al. 2015, *PCCP*, 17, 27281
- Turner, A. M., Bergantini, A., Abplanalp, M. J., et al. 2018, *Nat Commun*, 9, 3851
- Tarrago, G., Lacombe, N., Lévy, A., et al. 1992, *JMoSp*, 154, 30
- Villanueva, G.L., Cordiner, M., Irwin, P.G.J. et al. 2021, *NatAs*, 5, 631–635
- Vastel, C., Bottinelli, S., Caux, E., Glorian, J. -M., Boiziot, M., 2015, *Proceedings of the Annual meeting of the French Society of Astronomy and Astrophysics*, 313-316
- Ziurys, L. M., Savage, C., Highberger, J. L., et al. 2002, *ApJ*, 564, L45
- Ziurys, L. M., Schmidt, D. R., & Bernal, J. J. 2018, *ApJ*, 856, 169